nature communications

Article

https://doi.org/10.1038/s41467-025-60076-x

An in-situ assembled cobweb-like adhesive with high processability

Received: 1 December 2024

Accepted: 12 May 2025

Published online: 26 May 2025

Check for updates

Xiaoming Xie[1,2,4], Runhan Li[2,4], Yongsheng Qiao[1,4], Jiaqi Zhang[3], Zilin Zhang[1], Xingyu Xu[1], Jie Yang[1], Yan-Yu Peng[2], Yifa Chen[2] ✉, Shun-Li Li[2] & Ya-Qian Lan[2] ✉

Low temperature tolerant adhesive with high flexibility and adhesion strength is highly desired yet challenging owing to the presence of obvious volume shrinkage, increased brittleness, and reduced transmission of mechanical stress at low temperature. Inspired by the cobweb, we hereby develop a kind of flexible adhesive that can be used at low temperature by in-situ polymerization of disulfide bond-based polymer with polyoxometalate. This low-temperature tolerant adhesive presents high flexibility and adhesion strength, good processability and reversible adhesion ability, a wide tolerable temperature range (i.e., −196 to 50 °C), and a long-lasting adhesion effect (>80 days, −196 °C) that is significantly better than commercial solvent-free adhesives. The adhesive can be processed into high-strength cobwebs, injected into tiny tube models, and adhered onto complicated interfaces. Notably, it enables to be kilogram-scale produced through a solvent-free method, holding promise for potential utilization in fields like repairing artifacts or precision instruments with micro-fractures at low temperature.

Binding requirements in fields like precision instruments, cultural artifacts, soft robots or wearable devices, especially for the repairing of some micro-fractures in inaccessible positions, call for processable and robust adhesives to maintain the functions and properties in a cost-effective and convenient way[1–3]. At the same time, under harsh conditions like low temperature, it is highly desired yet scarce to develop powerful adhesives[4–8] with viscosity, processability, as well as low temperature tolerance. Nowadays, the traditional low-temperature adhesion is commonly utilized by commercial hot melt adhesives, such as ethylene-vinyl acetate copolymer (EVA), polyamide (PA), and polyurethane (PUR), etc[9–12]. Nevertheless, the temperature tolerance of these polymer-based hot melt adhesives is limited to around −50 °C, and their flexibility and adhesion strength would be drastically reduced at low temperatures, owing to the existence of some shortcomings such as low adhesion strength, embrittlement, and debonding in a low temperature environment[11,13–15]. Cobweb, a marvelous biological material with extraordinary strength, flexibility and viscoelasticity, has attracted the intense attention of researchers in the past few decades. These outstanding properties are mainly ascribed to the primary and secondary structures of spidroin, such as composition and arrangement of amino acids offering excellent viscosity, as well as strong interaction from massive β-sheet and α-helix assembly, offering strong strength and flexibility[16–19]. Inspired by nature, developing a new biomimetic material with excellent properties will be much necessary for the speedy development and ever-increasing demand of processable adhesives with low temperature resistance[20–22].

The intrinsic reason for the flexibility of polymers is that the atoms or groups in the chain can internally rotate around the covalent bond, which will generate different conformations in space[23,24], resulting in different degrees of curliness. In addition to this, the rotation or bending effects, due to the existence of non-covalent bonds (e.g., hydrogen bonds) that can induce changeable bond length or bond angle under external stimuli, can endow polymers with dynamic self-

[1]Department of Chemistry, Xinzhou Normal University, Xinzhou, Shanxi, China. [2]Guangdong Provincial Key Laboratory of Carbon Dioxide Resource Utilization, School of Chemistry, South China Normal University, Guangzhou, China. [3]Department of Mechanical and Aerospace Engineering, University of Missouri, Columbia, MI, USA. [4]These authors contributed equally: Xiaoming Xie, Runhan Li, Yongsheng Qiao. ✉e-mail: chyf927821@163.com; yqlan@m.scnu.edu.cn

adaptation[25–28]. In view of the flexibility nature of polymers, functional agents that can provide abundant non-covalent bonds and reduce the internal rotation barrier of the polymer would be desired to be introduced to endow the target polymer-based complex with both viscosity and flexibility at low temperature[21,29]. Aiming at this target and screening the polymer types, rubber polymers, containing S-S bonds with lower energy barrier for rotation around S-S axis than C-C axis, would be a kind of ideal matrix that might exhibit good flexibility at low temperature, due to the lower energy barrier for rotation around S-S axis than C-C axis[30,31]. Besides, as a kind of functional agents carrying multiple hydrogen protons and oxygen-rich surface, polyoxometalates (POMs)[32–36] would enable to form abundant hydrogen bonds with rubber polymers to synergistically integrate high viscosity with high flexibility, achieving a functional complex like cobweb[37–39]. Meanwhile, the insertion of spatial POMs has proven to reduce the cross-linking density of polymers and internal rotation barrier of chemical bonds, thus might facilitate the relaxation of rubber polymer chains, weaken residual stress, and increase flexibility of the rubber polymers[11,40,41]. If it can be processed under solvent-free conditions[42], low temperature resistance could also be integrated, achieving a kind of interesting and strong cobweb-like adhesive with combined functions of viscosity, flexibility, and low temperature resistance. Such interesting materials would be of broad interest in material science fields and have great potential in related applications under specific circumstances, while no related works have been reported as far as we know.

Here, we have fabricated a type of cobweb-inspired $H_4SiW_{12}O_{40}$ (SiW_{12}) based solvent-free polymer (CSSP) adhesive with high flexibility and ultra-low temperature resistance via an in-situ assembly method (Fig. 1), which can be facilely scale-up manufactured on a kilogram scale. The CSSP adhesive shows high adhesion strength at ultra-low temperature, good interface affinity for different substrates, and favorable long-range stability. This work may promote the development of flexible adhesives working at ultra-low temperatures for potential utilization in fields repairing artifacts or precision instruments with micro-fractures.

Results and discussion

Synthesis and characterizations of the CSSP adhesive

The solvent-free CSSP adhesive is facilely prepared through the in-situ polymerization (ROP) and assembly between thioctic acid (TA) monomer and SiW_{12} under a heat-assisted process (Supplementary Fig. 1, detail see Methods). Fourier-transform infrared (FT-IR) spectra (Fig. 2a and Supplementary Figs. 2, 3) confirm that the characteristic peaks (e.g., W = O_d, Si-O_a, W-O_b-W, and W-O_c-W) of SiW_{12} are still clearly discernible in CSSP adhesive, indicating the retained structure of SiW_{12} within the CSSP adhesive matrix. Moreover, the appearance of a new peak at 3508 cm^{-1} reveals the presence of hydrogen bonds[43], meanwhile a slight shift for the carbonyl group (C = O) in TA is observed from 1693 to 1705 cm^{-1} after forming CSSP adhesive, which is ascribed to possible hydrogen-bonding interaction[44]. Additionally, the powder X-ray diffraction (PXRD) confirms an amorphous feature of CSSP adhesive (Fig. 2b), which is different from SiW_{12} and TA, or even poly(thioctic acid) (PTA) (Supplementary Fig. 4). Besides, ^{13}C nuclear magnetic resonance (^{13}C NMR) and ^{1}H NMR spectra (Fig. 2c and Supplementary Figs. 5 to 8) verify the conversion of TA monomer into PTA polymer in producing CSSP adhesive[45,46]. The proton signal is widened and slightly shifted to low field for CSSP adhesive when compared with TA, possibly due to the existence of intermolecular hydrogen bonds[47,48]. Simultaneously, the Raman spectroscopy shows that the distinctive peak of disulfide bonds notably shifts from 511 to 525 cm^{-1}, proving the occurrence of transformation from cyclic disulfides of TA monomer into linear disulfides of CSSP adhesive[49] (Fig. 2d and Supplementary Fig. 9).

Furthermore, matrix-assisted laser desorption ionization time-of-flight mass spectra (MALDI-TOF-MS) reveals the presence of linear polymer (Mn, ~3032) in CSSP adhesive, suggesting the success of ring opening polymerization through the heat-assisted process[50] (Fig. 2e and Supplementary Fig. 10). Moreover, ^{29}Si NMR (Fig. 2f) spectra display that the chemical shift (−85.47 ppm) of Si element in CSSP adhesive is almost the same with that of SiW_{12} (−85.53 ppm), verifying the remained Keggin-type structure of SiW_{12} within the CSSP adhesive matrix. Additionally, the W 4*f*, S 2*p* and C 1*s* signals are explicitly detected by X-ray photoelectron spectroscopy (XPS) (Supplementary

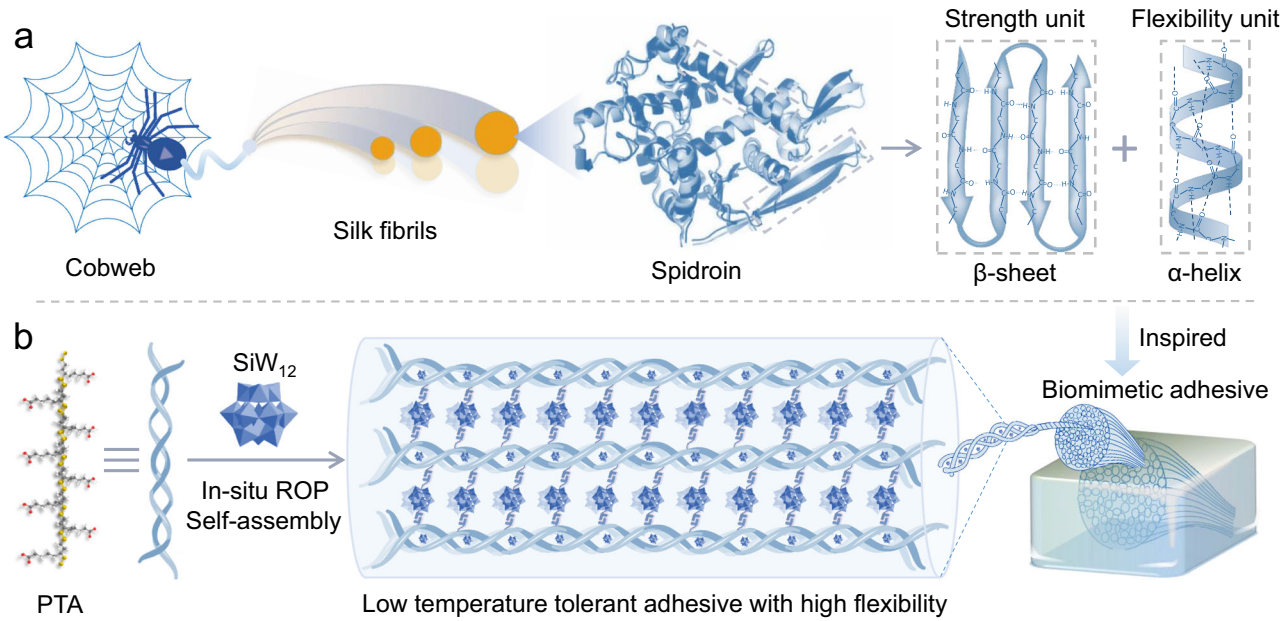

Fig. 1 | Schematic illustration of low temperature tolerant adhesive with high flexibility inspired by cobweb. a The silk fibrils in cobweb with abundant β-sheet and α-helix secondary structures (the structure of spidroin is from public domain (RCSB PDB) without copyright restrictions (Yang, K. K., Yeh, H., & Zanichelli, N. (2022). Masked inverse folding with sequence transfer for protein representation learning (1.0). Zenodo. https://doi.org/10.1234/mifst)). **b** Schematic representation of CSSP adhesive.

https://doi.org/10.1038/s41467-025-60076-x

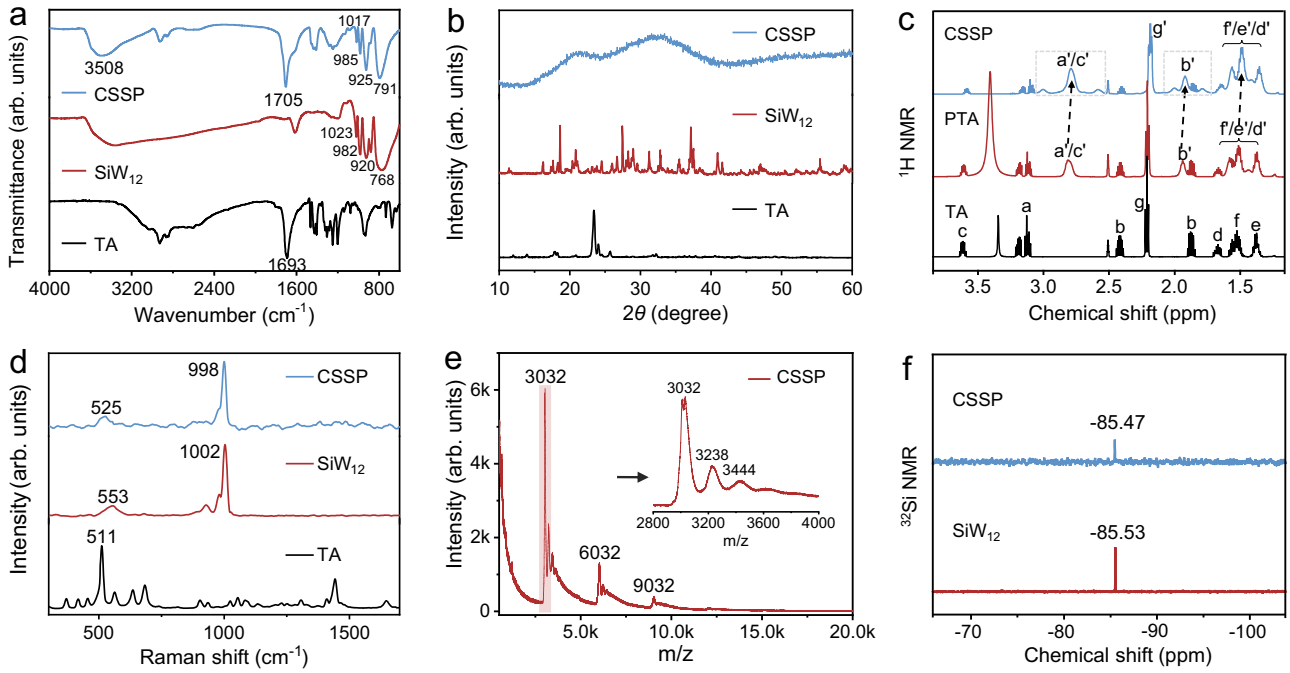

Fig. 2 | Characterizations of the CSSP adhesive. a FTIR spectra of CSSP adhesive, SiW_{12}, and TA. **b** PXRD patterns of CSSP adhesive, SiW_{12}, and TA. **c** ^{1}H NMR spectra of CSSP adhesive, PTA and TA in DMSO-d_6 (500 MHz). **d** Raman spectra of CSSP adhesive, SiW_{12}, and TA. **e** MALDI-TOF-MS spectrum of CSSP adhesive. **f** ^{32}Si NMR spectra of CSSP adhesive and SiW_{12} in DMSO-d_6 (500 MHz).

Fig. 11). The appearance of W^{5+} ($4f_{7/2}$ and $4f_{5/2}$) indicates the occurrence of charge transfer between PTA and SiW_{12} (Supplementary Fig. 12), which is further verified by diffuse reflectance UV-vis absorption due to the additional strong and broad absorption at $\lambda > 500$ nm for CSSP adhesive (Supplementary Fig. 13). The S 2*p* spectrum of CSSP adhesive includes two peaks of disulfide peak at 164.55 eV and aliphatic organosulfur peak at 163.31 eV (Supplementary Fig. 14), implying the occurrence of ring-opening polymerization of disulfide bonds on the five-membered ring of TA monomer[43]. Meanwhile, the increased intensity of C-O bonds in CSSP adhesive confirms the possibility of hydrogen bonds[51] (Supplementary Fig. 15). Scanning electron microscope (SEM) and energy-dispersive X-ray spectroscopy (EDS) element mapping tests are carried out to characterize the morphology of CSSP adhesive. The results show that CSSP adhesive exhibits flat and dense surfaces, and different elements from SiW_{12} and TA are evenly distributed in CSSP adhesive (Fig. 3a and Supplementary Fig. 16).

Adhesive materials with high mechanical strength and long-term stability play a crucial role in the practical application process[52]. Satisfyingly, the CSSP adhesive attached to the SS substrate can facilely lift a weight of ~60 kg (Fig. 3b), suggesting its favorable adhesion property. Moreover, this adhesive can also tolerate a weight of 2 kg for 100 days (Supplementary Fig. 17), implying the strong and long-lasting adhesion behaviors of the CSSP adhesive. Additionally, the CSSP adhesive is capable of achieving kilogram preparation. The raw materials of this adhesive are easily available, and it is expected to further reduce production costs when it is produced on a large scale (Fig. 3b). In comparison with PTA, the CSSP adhesive exhibits higher viscosity at temperature below 50 °C as presented in the viscosity tests (Fig. 3c). The gradually decreased viscosity is accompanied by high liquidity with increasing temperature, which will facilitate spreading and adhesion on substrates. Besides, the CSSP adhesive can be readily adhered onto different substrates including artificial and natural materials (Supplementary Fig. 18). Subsequently, the quantitative adhesion strength is tested by a lap-shear joint method. As a result, the CSSP adhesive exhibits high adhesive performances on stainless steel (SS, 3.5 MPa), aluminum (Al, 3.2 MPa), and glass (2.8 MPa) due to strong chemical bonds and mechanical interlocking with substrates[53], which is comparable to most of reported solvent-free adhesives (Supplementary Table 1). Contrastively, the bonding strengths are relatively weaker on polyetheretherketone (PEEK), polypropylene (PP) and polytetrafluoroethylene (PTFE) substrates with lower surface energy (Fig. 3d). Noticeably, the admirable adhesion capacity surpasses almost all of POMs-based adhesives reported nowadays (Supplementary Fig. 19 and Supplementary Table 2). The adhesion time is also examined, and the result shows that the adhesion strength of CSSP adhesive could reach maximum within 10 min for SS substrate (Supplementary Fig. 20). Additionally, we screen a series of advanced adhesives, namely solvent-free EVA, TPU, double-sided tape, and solvent-based 3 M instant adhesive, for the purpose of comparing their shear strengths with that of CSSP adhesive. Notably, the shear strength of CSSP adhesive is comparable or greater than currently available commercial adhesives, such as solvent-free TPU (~4.81 MPa), EVA (~3.13 MPa), double-sided tape (DST, ~0.35 MPa) and solvent-based 3 M instant adhesive (~1.93 MPa) (Supplementary Fig. 21). Furthermore, there is no significant weakening of adhesion strength for the CSSP adhesive after undergoing 20 cycles of adhesion and deadhesion through simple heating and cooling treatments (Fig. 3e). In addition, the adhesion failure after detachment primarily occurs in adhesive itself for SS substrate and interfacial adhesion for PTFE substrate (Supplementary Figs. 22 and 23), respectively, because the SS substrate has higher free energy and roughness than PTFE substrate[54,55].

Achieving both high toughness and flexibility for adhesive material is an indispensable and important property in the fields of flexible electronics industry and wearable devices[56]. Here, the CSSP adhesive can be drawn into longer fibers under the heat-assisted method, and be woven into a resembling cobweb (Fig. 3f), indicating its favorable toughness, flexibilit,y and processability. Furthermore, the CSSP adhesive can not only adhere to different materials (Supplementary Fig. 18), but also be injected into tiny glass tubes with different models (such as "I", "V", "Y" or even sophisticated "Love" model) (Fig. 4a-d), suggesting its favorable processability that can be potentially used to repair the local micro-fracture inside precision instruments through an

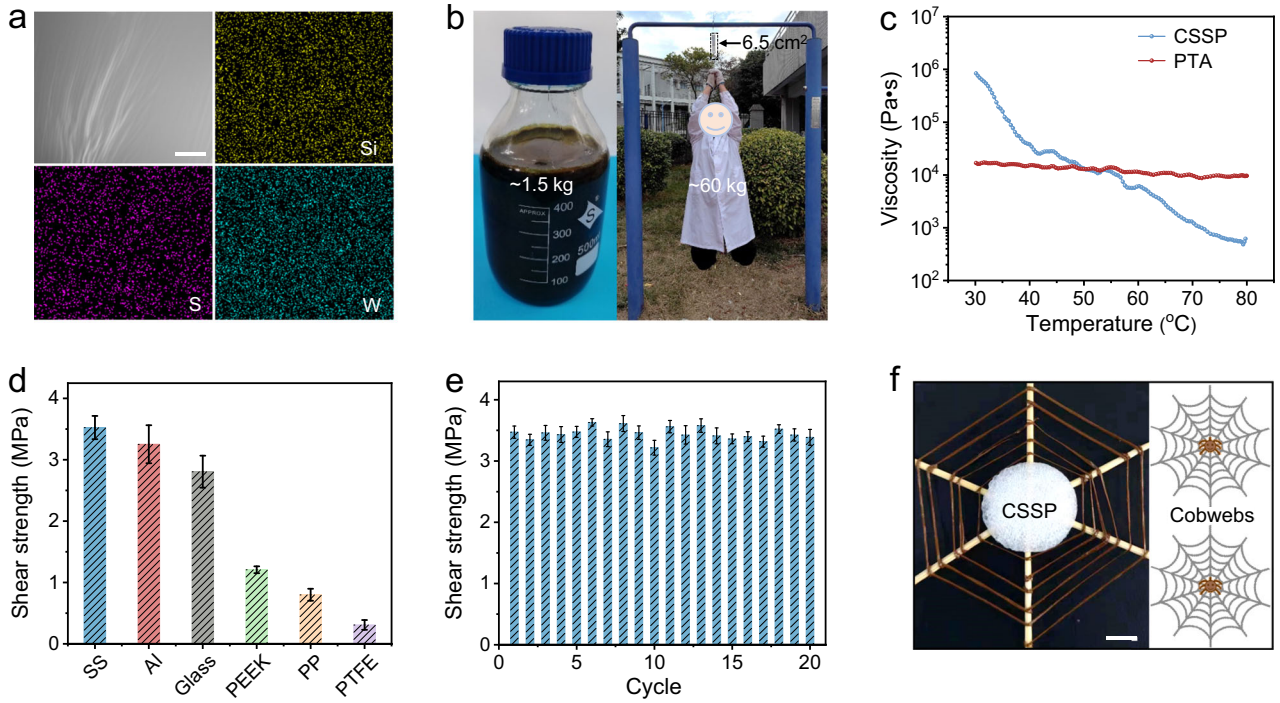

Fig. 3 | Morphology, flexibility, and mechanical property of the CSSP adhesive. **a** SEM and corresponding elemental mapping images of CSSP adhesive (scale bar, 20 μm). **b** Macroscopic photographs of CSSP adhesive obtained in kilogram scale and a weight of ~60 kg bonded by CSSP adhesive. **c** Shear viscosity of PTA and CSSP adhesive. **d** Shear strengths of CSSP adhesive on different substrates. **e** Cycling stability of CSSP adhesive. **f** A resembling cobweb woven using CSSP adhesive (scale bar, 2 cm). The error bars for **d**, **e** represent mean ± standard deviation ($n = 3$ independent samples).

injection bonding method. In addition, it is also suitable for the complicated interface bonding, like irregular glass or stone. The separated glass tubes can be easily adhered together into an integral shape by CSSP adhesive (Fig. 4e), which can be lifted easily without falling off. Simultaneously, the broken interface of a "Monkey King" statue in stone material can also be perfectly repaired by CSSP adhesive to maintain the original features, which can tolerate its own weight of ~500 g (Fig. 4f). These results demonstrate its distinctive repairing ability in complicated interface processing like artifacts or precision instruments with micro-fractures. The maintenance of good interfacial infiltration in extreme conditions like non-polar solvent environment is also an eye-catching trait for the adhesive[57]. To test the resistance to non-polar solvents, the CSSP adhesive is adhered to SS substrates and tested by soaking in some solvents, including mesitylene (TMB), dichlorobenzene (DCB), petroleum ether (PE), octanoic acid (OA), and cyclohexane (CYH). Strikingly, no separation occurs, and the shear strengths remain relatively stable after 15 days (Supplementary Figs. 24 and 25). In sharp contrast, a commercially available hot melt adhesive (EVA) displays negligible shear strength after soaking in mesitylene for 7 days (Supplementary Fig. 26). More interestingly, the CSSP adhesive is capable of preventing an emergency leakage for PE solvent (Supplementary Fig. 27 and Supplementary Movie 1). In addition, the resistance of CSSP adhesive to polar solvents like water or ethanol has been investigated through immersion experiments. The result shows that a minor amount of CSSP adhesive is dissolved after immersion in water (or ethanol) for 1 day at room temperature (Supplementary Figs. 28 and 29). Interestingly, the CSSP adhesive slightly becomes soft and partly transforms into a traditional solvent-assisted adhesive, owing to the interaction of water molecules (or ethanol) with adhesive that results in parts of the hydrogen-bonded networks in CSSP adhesive being collapsed and rebuilt. Meanwhile, the stability and viscosity of CSSP adhesive under different pH conditions (pH = 1, 7 and 14) are assessed (Supplementary Figs. 30 and 31). Moreover, the adhesion strengths of CSSP adhesive under varying relative humidity conditions (from 40% to 80%) have been tested, and the experimental results clearly indicate that the adhesion strengths of CSSP adhesive only have slight decrease with the increase of relative humidity (Supplementary Fig. 32), proving its good resistance to humidity.

Based on the above discussion, the SS substrate is chosen as a model to further assess the adhesion behavior and clarify mechanism of CSSP adhesive. It should be mentioned that the CSSP adhesive (mass ratio, TA: SiW_{12} = 1: 2) can exhibit the maximum viscosity and shear strength of 3.5 MPa on SS, which is significantly better than other mass ratios (1: 1, 2.7 MPa; 1: 3, 1.8 MPa) (Supplementary Figs. 33 and 34). Hence, the CSSP adhesive (mass ratio, TA: SiW_{12} = 1: 2) is chosen as a model sample for the following in-depth study. Noteworthy, the shear strength of CSSP adhesive obviously exceeds the SiW_{12}-based solvent-assisted adhesive (SSAA) (~ 30 times, Supplementary Figs. 35 and 36). As expected, an analogous adhesive (CPSP) based on $H_3PW_{12}O_{40}$ (PW_{12}) and PTA can also be obtained through a similar in-situ assembly method (Supplementary Fig. 37), which has been verified by various characterizations (Supplementary Figs. 38 to 40). The weaker shear strength of CPSP adhesive than CSSP adhesive might be due to the less protons of PW_{12} compared with SiW_{12}, which will reduce the cross-linked sites in the assembly process (Supplementary Figs. 41 and 42). Whereas, bulky materials with negligible viscosity are obtained when replacing PW_{12} with $Na_3PW_{12}O_{40}$ or replacing TA with Na-TA (Supplementary Fig. 43), indicative of the dominating role of protons in the formation of CSSP adhesive. Furthermore, we assess the effect of disulfide bonds on the formation of adhesives by replacing TA with octanoic acid (OA) (Supplementary Fig. 43). The result shows that no adhesive is observed, suggesting that disulfide bonds play a vital role in promoting the formation of adhesives.

Aside from high adhesion strength, the viscosity, energy storage, and loss modulus of CSSP adhesive have been evaluated by rheological characterization. Rheology tests show that the storage modulus (G′), loss modulus (G″), and complex viscosity (η*) of CSSP adhesive are inversely proportional to the environmental temperature (Fig. 5a and

https://doi.org/10.1038/s41467-025-60076-x

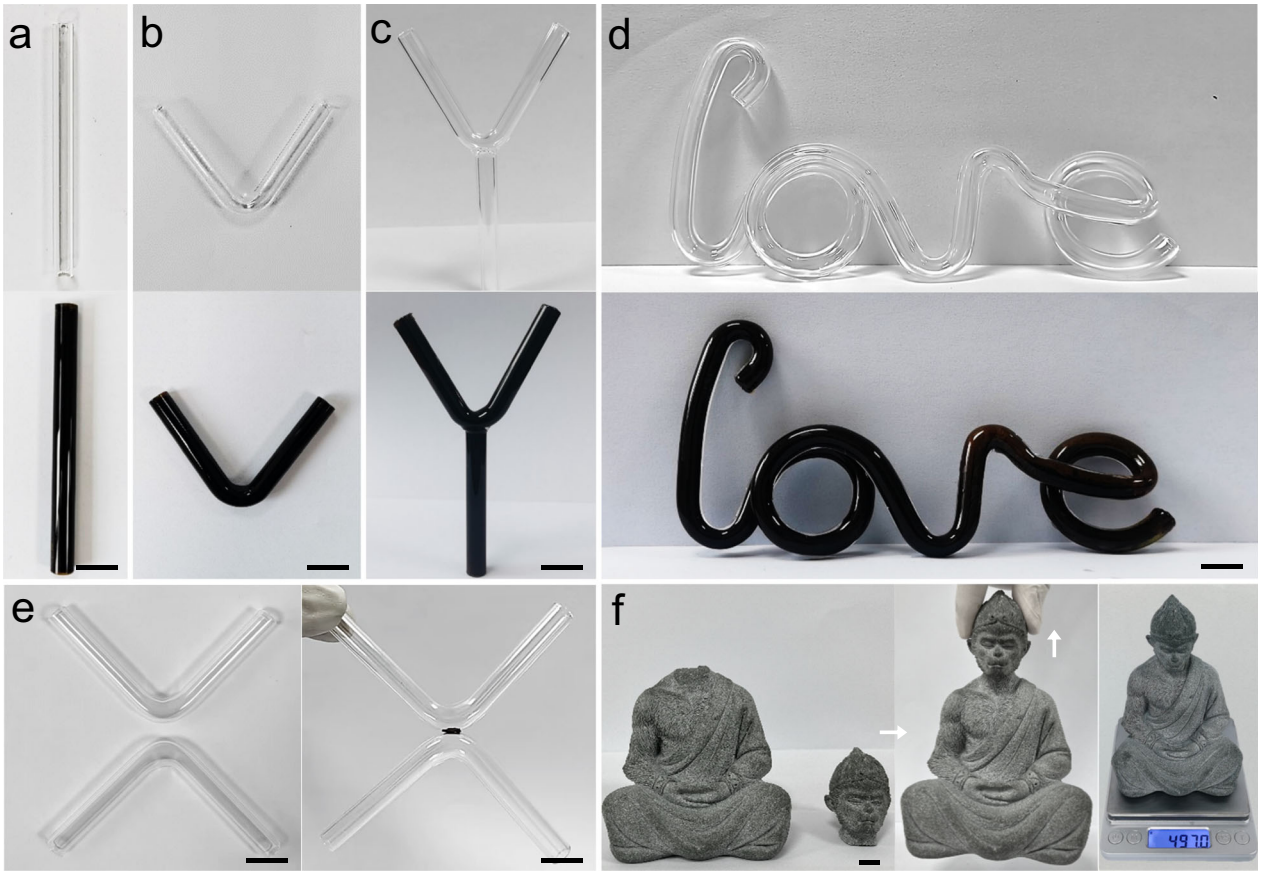

Fig. 4 | The processability and interfacial adhesion tests of CSSP adhesive (scale bar, 1 cm). **a**–**c** The images of transfusing the CSSP adhesive into different glass tube models. **d** The image of transfusing the CSSP adhesive into a sophisticated "Love" shape model. **e** The image of sticking scattered molds together into an integrated shape model. **f** The images of repairing a fractured "Monkey King" statue by CSSP adhesive.

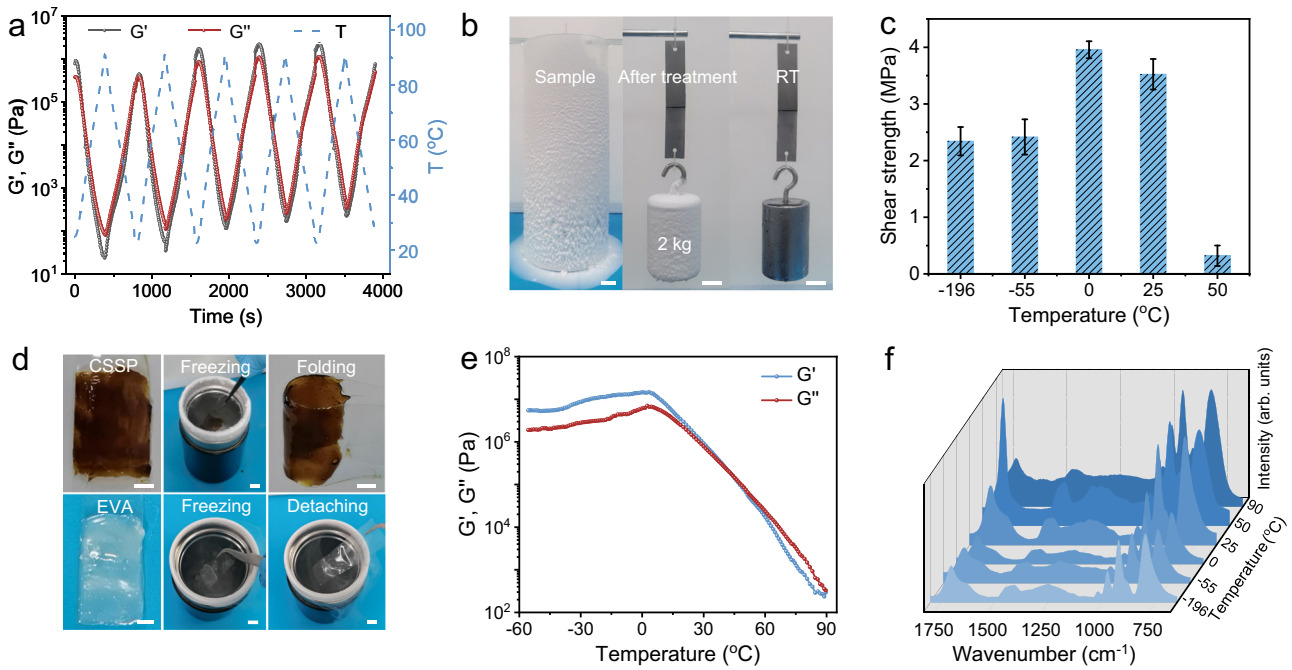

Fig. 5 | The behaviors of the CSSP adhesive under a wide temperature range. **a** The reversible curve of storage modulus (G′) and loss modulus (G″) of CSSP adhesive at cyclic temperature. **b** Macroscopic adhesion tests of CSSP adhesive in liquid nitrogen (scale bar, 2 cm). **c** Shear strengths of CSSP adhesive on SS substrates at various temperatures. **d** Macroscopic flexibility tests of CSSP adhesive and commercial solvent-free EVA adhesive at ultra-low temperature (scale bar, 1 cm). **e** Rheology measurements of CSSP adhesive between −60 and 90 °C. **f** Temperature-dependent FT-IR spectra of CSSP adhesive from −196 to 90 °C. The error bars for **c** represent mean ± standard deviation ($n = 3$ independent samples).

Supplementary Fig. 44). Actually, the G′ of CSSP adhesive is higher than G″ at below ~50 °C, demonstrating a gel-like or solid-like behavior[57]. Nevertheless, the G″ of CSSP adhesive exceeds the G′ at above ~50 °C, generating a viscosity-dominated state that is beneficial to the interface adhesion. Furthermore, the CSSP adhesive exerts reversible G′, G″, and η* with the operating temperature of the cycle between 20 and 90 °C, which is probably due to the solvent-free property and reversible hydrogen-bonding interaction.

Low temperature-resistance and flexibility properties

At present, most adhesives tend to shrink, become brittle, and detach, owing to the lack of flexibility and tolerance at lower temperature[20]. Therefore, it is still challenging and highly desired to develop flexible adhesives with ultra-low temperature tolerance ability. The thermogravimetric analysis (TGA) and differential scanning calorimeter (DSC) measurements show that the CSSP adhesive has a lower glass transition temperature (T_g) of -2.1 °C compared to that of TA (61.9 °C) and PTA (53.1 °C) (Supplementary Figs. 45 to 47), indicating its better flexibility at relatively low temperature. Noteworthy, the two SS slices bonded using CSSP adhesive can carry a weight of 2 kg under liquid nitrogen conditions, and still keep the original state when the surrounding environment returns to room temperature (Fig. 5b and Supplementary Movie 2). In stark contrast, the EVA adhesive adhered between two SS slices will be broken instantly after immersing in liquid nitrogen (Supplementary Fig. 48) owing to the existence of obvious volumetric contraction and enhanced fragileness (Supplementary Figs. 49 and 50). Then, the shear strength of CSSP adhesive is monitored at different temperatures. The shear strength of CSSP adhesive is negligible at 50 °C, and will gradually increase to a maximum value of ~3.9 MPa at 0 °C (Fig. 5c). After that, the shear strength decreases to ~2.3 MPa at −196 °C. It is worth noting that the shear strength of CSSP adhesive can still remain stable despite being immersed in liquid nitrogen for 80 days (Supplementary Fig. 51), implying good ultra-low temperature tolerance and significantly better than commercial EVA. To further verify the adhesion performance of CSSP adhesive for the complicated interface at low temperature, the repaired "Monkey King" statue mentioned above is immersed in liquid nitrogen, and no fracture at the damaged interface is observed after treatment (Supplementary Fig. 52 and Supplementary Movie 3), proving its ability in repairing the complicated interface under ultra-low temperature.

In addition, to test the flexibility at low temperature, the CSSP adhesive is coated on soft PE substrate, then immersed in liquid nitrogen for ~60 s. After placing it in air for ~15 s, the CSSP adhesive can still be folded multiple times (Fig. 5d and Supplementary Movie 4). No separation or rupture phenomenon is observed after repeating the procedure of freezing-folding-freezing, suggesting admirable flexibility at ultra-low temperature. However, the EVA adhesive tends to fracture and fall off from PP substrate at low temperature (Fig. 5d and Supplementary Movie 4). Additionally, we further examine the low-temperature rheology of CSSP adhesive, which exhibits relatively stable G′ and G″ over a wide temperature range from −60 to 0 °C (Fig. 5e), indicative of good tolerance toward low temperature. Besides, the temperature-dependent FT-IR spectra of CSSP adhesive (Fig. 5f, Supplementary Figs. 53 and 54) show negligible change in the characteristic peaks of both TA and SiW_{12}, and evident signals of H-bond at below 50 °C, indicating that the interactions in CSSP adhesive remain almost intact over a wide temperature range.

The adhesion mechanism based on CSSP adhesion with favorable adhesion properties is further investigated through theoretical calculations. Generally, the adhesion ability of adhesive materials depends on two main factors, including cohesion and interfacial adhesion effects[31,41,58]. Whereas most adhesion mechanisms based on theoretical calculations mainly focus on the simulation at room temperature, it is still rare to study both cohesion and interfacial adhesion effects at low temperature. Thus, the density functional theory (DFT) calculations are performed to investigate the CSSP adhesive at the molecular level. The results display that the interaction energy between PTA and SiW_{12} is -107.53 kJ/mol (Fig. 6a, Supplementary Figs. 55 to 57), suggesting that the binding stability between PTA and SiW_{12} will be obviously strengthened through hydrogen-bonding interaction. Thus, the interweavement of SiW_{12} into PTA networks can result in the formation of a stable CSSP adhesive. Additionally, the molecular dynamics (MD) simulation is carried out to further evaluate the temperature-dependent interaction energy. The average interaction energy between PTA and SiW_{12} at 25 °C is −3229 kJ/mol in the model system at 5 ns (Fig. 6b and Supplementary Fig. 58). Besides, there exist significant fluctuations of the interaction energy at 50 °C and decreases to −3075 kJ/mol (Supplementary Figs. 59 and 60). Noteworthy, the interaction energy at −196 °C rapidly reaches equilibrium and holds steady, and the significantly enhanced interaction energy remains at −3420 kJ/mol (Fig. 6b, d). The high interaction energy can endow CSSP adhesive with large energy dissipation when dragging the adhesive due to the existence of strong hydrogen-bonding interaction, which might also be the main factors for CSSP adhesive to display favorable adhesion and flexibility at ultra-low temperature. In sharp contrast, the interaction energy is obviously reduced to -2661 kJ/mol after replacing SiW_{12} with PW_{12} because of the fewer protons provided by PW_{12} to interact with PTA (Supplementary Figs. 61 and 62). In addition, the interfacial adhesion effect is further evaluated using MD simulations. The interaction energy between CSSP adhesive and SS substrate (Supplementary Data 1) at 25 °C is average −15,752 kJ/mol in the model system at 2 ns (Fig. 6c and Supplementary Movie 5). There is a slight decrease (−14,977 kJ/mol) in the interaction energy at 50 °C (Supplementary Fig. 63 and Supplementary Movie 6). It is worth noting that the average interaction energy at −196 °C obviously increases to -17684 kJ/mol (Fig. 6c, e and Supplementary Movie 7), indicating its good mechanical force transmission across the substrate and good interfacial adhesion property at ultra-low temperature.

Inspired by the cobweb, we have developed a type of POMs based low-temperature adhesive with flexibility through the in-situ polymerization of disulfide bond-based polymer with polyoxometalate. The obtained CSSP adhesive exhibits high flexibility and adhesion strength, favorable processability and reversible adhesion ability, a wide tolerable temperature range (i.e., −196 to 50 °C), and a long-lasting adhesion effect (>80 days, −196 °C) that is significantly better than commercial solvent-free adhesives. Meanwhile, the adhesive can be processed into high-strength cobwebs, injected into tiny tube models, and adhered onto complicated interfaces. Noteworthy, it enables to be kilogram-scale produced through a facile solvent-free processing method. This work may provide a strategy to explore low-temperature-tolerant adhesives with high flexibility that can meet the stringent requirements under complicated working conditions.

Methods

Materials

All solvents and reagents obtained from commercial sources were used without further purification. TA (99%) and Na-TA (98%) were bought from Macklin Biochemical Technology Co., Ltd. (Shanghai). SiW_{12} (99%), PW_{12} (98%), and $Na_3PW_{12}O_{40}$ (99%) were purchased from Aladdin Industrial Corporation. Mesitylene (97%), dichlorobenzene (98%), cyclohexane (99.7%), petroleum ether (≥95%), methyl alcohol (≥99.9%), and octanoic acid (≥99%) were obtained from Shanghai Titan Scientific Co., Ltd. The EVA (18 wt.%) adhesive was bought from Huizhou Hengwang Hardware Plastic Co., Ltd.

Syntheses of the CSSP adhesive with different mass ratios (1: 1, 1: 2 and 1: 3)

The POMs based low temperature tolerant adhesives with high flexibility were prepared using a simple in-situ assembly method. TA (1 g) and SiW_{12} (1, 2, and 3 g) were evenly mixed, then heated at 90 °C for 2 h.

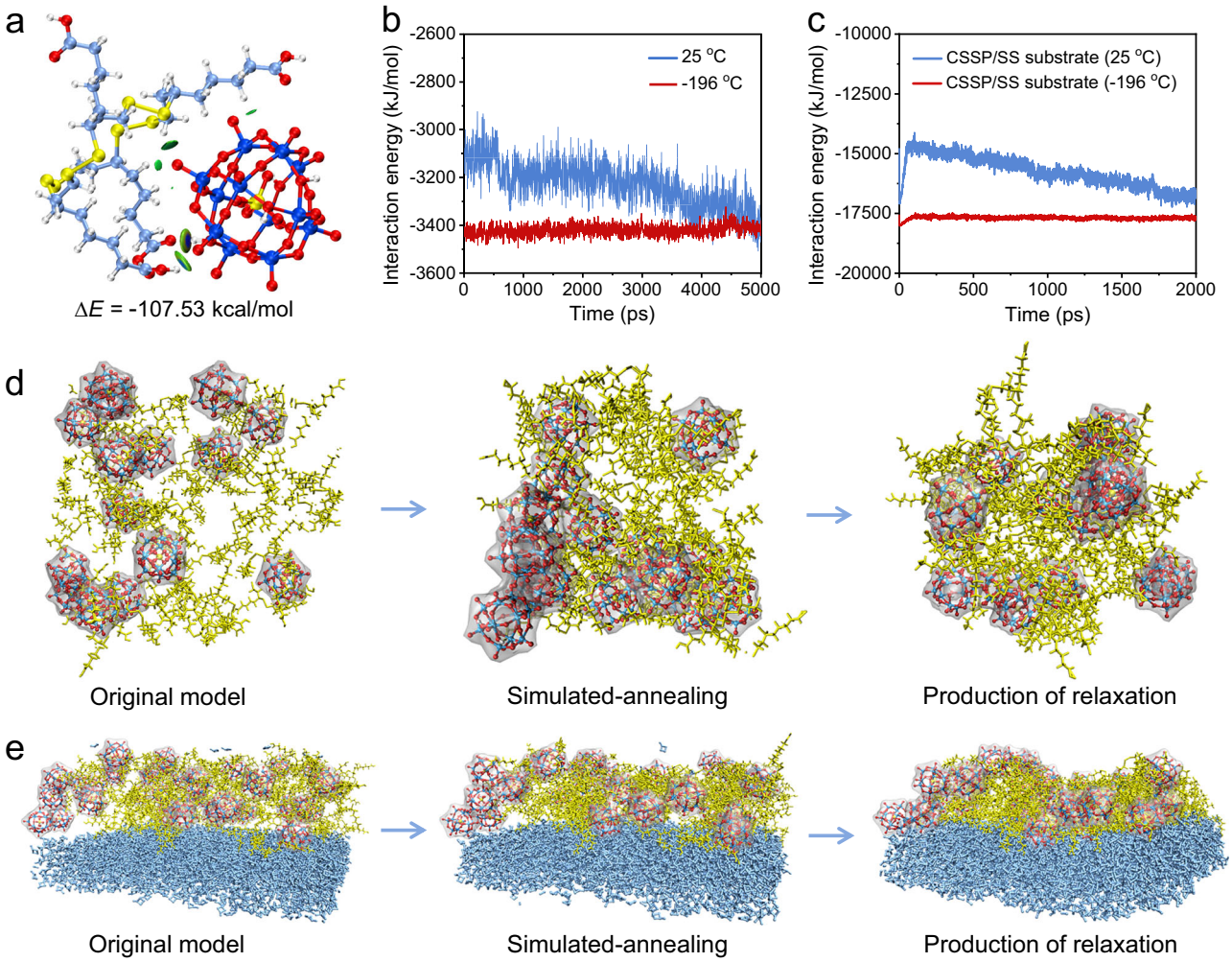

Fig. 6 | Theoretical calculations for the interaction between SiW_{12} and PTA. **a** Independent gradient model based on Hirshfeld partition (IGMH) isosurfaces for the interaction energy between SiW_{12} and PTA. **b** The interaction energy between PTA and SiW_{12} at 25 and −196 °C for the final 5 ns in the MD simulation. **c** The interaction energy between CSSP adhesive and SS substrate at 25 and −196 °C for the final 2 ns in the MD simulation. **d** The configurations of molecular models of SiW_{12} and PTA at −196 °C. **e** The configurations of molecular models of CSSP adhesive and SS substrate at −196 °C.

The cobweb-inspired SiW_{12}-based solvent-free polymer (CSSP) adhesive was obtained after cooling to room temperature. The CSSP adhesive can also be prepared on a kilogram scale by increasing raw materials in equal proportions. As a contrast, another cobweb-inspired PW_{12}-based solvent-free polymer (CPSP) adhesive was obtained by replacing SiW_{12} with PW_{12} under a similar preparation method. In addition, The SiW_{12}-based solvent-assisted adhesive (SSAA) was prepared by heating the mixture of SiW_{12} and TA in methyl alcohol for 30 min (TA: SiW_{12} = 1: 2; 90 °C).

Data availability

All data that support the findings of this study are available within the paper and its supplementary information files or are available from the corresponding authors upon request. Source data and coordinate files for computational measurements are provided with this paper. Source data are provided with this paper.

References

1. Westerman, C. R., McGill, B. C. & Wilker, J. J. Sustainably sourced components to generate high-strength adhesives. *Nature* **621**, 306–311 (2023).
2. Yang, G., Gong, Z., Luo, X., Chen, L. & Shuai, L. Bonding wood with uncondensed lignins as adhesives. *Nature* **621**, 511–515 (2023).
3. Hwang, D. et al. Metamaterial adhesives for programmable adhesion through reverse crack propagation. *Nat. Mater.* **22**, 1030–1038 (2023).
4. Nepal, D. et al. Hierarchically structured bioinspired nanocomposites. *Nat. Mater.* **22**, 18–35 (2023).
5. Sun, L. et al. Spider-silk-inspired tough, self-healing, and melt-spinnable ionogels. *Adv. Sci.* **11**, e2305697 (2024).
6. Fu, Q., Hao, S., Meng, L., Xu, F. & Yang, J. Engineering self-adhesive polyzwitterionic hydrogel electrolytes for flexible zinc-ion hybrid capacitors with superior low-temperature adaptability. *ACS Nano* **15**, 18469–18482 (2021).
7. Wang, Y. et al. Spider silk-inspired binder design for flexible lithium-ion battery with high durability. *Adv. Mater.* **35**, 2303165 (2023).
8. Zhao, W. et al. Neuron-inspired sticky artificial spider silk for signal transmission. *Adv. Mater.* **35**, 2300876 (2023).
9. Skeist, I. *Handbook of adhesives*, (Van Nostrand Reinhold Co., 1977).
10. Awaja, F., Gilbert, M., Kelly, G., Fox, B. & Pigram, P. J. Adhesion of polymers. *Prog. Polym. Sci.* **34**, 948–968 (2009).
11. Chen, J. et al. Ultra-strong and proton conductive aqua-based adhesives from facile blending of polyvinyl alcohol and tungsten oxide clusters. *Adv. Funct. Mater.* **32**, 2111892 (2022).
12. Pietron, J. J. & Mirkarimi, P. B. Review of the effects of polymer binder properties on microstructure and irreversible volume

growth of plastic bonded explosives formulations. *Propellants Explos., Pyrotech.* **47**, e202100379 (2022).
13. Chen, M. et al. Fast, strong, and reversible adhesives with dynamic covalent bonds for potential use in wound dressing. *Proc. Natl Acad. Sci.* **119**, e2203074119 (2022).
14. Marques, E. A. S., da Silva, L. F. M., Banea, M. D. & Carbas, R. J. C. Adhesive joints for low- and high-temperature use: an overview. *J. Adhes.* **91**, 556–585 (2015).
15. Srinivasan, D. V. & Idapalapati, S. Review of debonding techniques in adhesively bonded composite structures for sustainability. *Sustain. Mater. Technol.* **30**, e00345 (2021).
16. Yarger, J. L., Cherry, B. R. & van der Vaart, A. Uncovering the structure-function relationship in spider silk. *Nat. Rev. Mater.* **3**, 18008 (2018).
17. Cranford, S. W., Tarakanova, A., Pugno, N. M. & Buehler, M. J. Nonlinear material behaviour of spider silk yields robust webs. *Nature* **482**, 72–76 (2012).
18. Nova, A., Keten, S., Pugno, N., Redaelli, A. & Buehler, M. Molecular and nanostructural mechanisms of deformation, strength and toughness of spider silk fibrils. *Nano. Lett.* **10**, 2626–2634 (2010).
19. Li, J. et al. Spider silk-inspired artificial fibers. *Adv. Sci.* **9**, e2103965 (2022).
20. Ling, S. et al. Polymorphic regenerated silk fibers assembled through bioinspired spinning. *Nat. Commun.* **8**, 1387 (2017).
21. Liu, X. et al. A spider-silk-inspired wet adhesive with supercold tolerance. *Adv. Mater.* **33**, 2007301 (2021).
22. Zhang, J. et al. Electrothermal dry adhesives with high adhesion under low temperatures based on tunable stiffness. *Adv. Funct. Mater.* **34**, 2309800 (2024).
23. Gedde, U. W. *Polymer Physics*, (Springer Netherlands, Dordrecht, 1999).
24. Xu, Z., Hadjichristidis, N., Fetters, L. J. & Mays, J. W. Structure/chain-flexibility relationships of polymers. *Phys. Prop. Polym.* **120**, 1–50 (1995).
25. Yang, Y. & Urban, M. W. Self-healing polymeric materials. *Chem. Soc. Rev.* **42**, 7446–7467 (2013).
26. Yang, P. et al. Stimuli-responsive polydopamine-based smart materials. *Chem. Soc. Rev.* **50**, 8319–8343 (2021).
27. Yao, G., Li, F. & Dong, S. Solvent-free bulk soft material with low-temperature tolerance: Transparency, flexibility, stretchability, and adhesion. *Chem. Eng. Sci.* **281**, 119164 (2023).
28. Meng, Q., Huang, Y., Li, L., Wu, F. & Chen, R. Smart batteries for powering the future. *Joule* **8**, 344–373 (2024).
29. Li, Z. et al. Healable and recyclable elastomers with record-high mechanical robustness, unprecedented crack tolerance, and superhigh elastic restorability. *Adv. Mater.* **33**, 2101498 (2021).
30. Steudel, R. & Chivers, T. The role of polysulfide dianions and radical anions in the chemical, physical and biological sciences, including sulfur-based batteries. *Chem. Soc. Rev.* **48**, 3279–3319 (2019).
31. Wang, S. et al. Polymer-based dielectrics with high permittivity and low dielectric loss for flexible electronics. *J. Mater. Chem. C.* **10**, 6196–6221 (2022).
32. Vilà-Nadal, L. & Cronin, L. Design and synthesis of polyoxometalate-framework materials from cluster precursors. *Nat. Rev. Mater.* **2**, 17054 (2017).
33. Gumerova, N. I. & Rompel, A. Synthesis, structures and applications of electron-rich polyoxometalates. *Nat. Rev. Chem.* **2**, 0112 (2018).
34. Moussawi, M. A. et al. Polyoxometalate, cationic cluster, and γ-cyclodextrin: from primary interactions to supramolecular hybrid materials. *J. Am. Chem. Soc.* **139**, 12793–12803 (2017).
35. Anyushin, A. V., Kondinski, A. & Parac-Vogt, T. N. Hybrid polyoxometalates as post-functionalization platforms: from fundamentals to emerging applications. *Chem. Soc. Rev.* **49**, 382–432 (2020).
36. Cameron, J. M. et al. Supramolecular assemblies of organo-functionalised hybrid polyoxometalates: from functional building blocks to hierarchical nanomaterials. *Chem. Soc. Rev.* **51**, 293–328 (2022).
37. Peng, Q. et al. Adhesive coacervates driven by hydrogen-bonding interaction. *Small* **16**, 2004132 (2020).
38. Misra, A., Kozma, K., Streb, C. & Nyman, M. Beyond charge balance: counter-cations in polyoxometalate chemistry. *Angew. Chem. Int. Ed.* **59**, 596–612 (2020).
39. Zhang, S., Shi, W. & Wang, X. Locking volatile organic molecules by subnanometer inorganic nanowire-based organogels. *Science* **377**, 100–104 (2022).
40. Alves, L. S. et al. PEG-infiltrated polyoxometalate frameworks with flexible form-factors. *ACS Mater. Lett.* **4**, 1937–1943 (2022).
41. Zhang, S., Shi, W., Yu, B. & Wang, X. Versatile inorganic sub-nanometer nanowire adhesive. *J. Am. Chem. Soc.* **144**, 16389–16394 (2022).
42. Xie, X. et al. A solvent-free processed low-temperature tolerant adhesive. *Nat. Commun.* **15**, 5017 (2024).
43. Chen, C. et al. Tannic acid-thioctic acid hydrogel: a novel injectable supramolecular adhesive gel for wound healing. *Green. Chem.* **23**, 1794–1804 (2021).
44. Dang, C. et al. Polyfunctional and multisensory bio-ionoelastomers enabled by covalent adaptive networks with hierarchically dynamic bonding. *Adv. Mater.* **2406967** (2024).
45. Zhang, Q. et al. Exploring a naturally tailored small molecule for stretchable, self-healing, and adhesive supramolecular polymers. *Sci. Adv.* **4**, eaat8192 (2018).
46. Pal, S. et al. Recyclable surgical, consumer, and industrial adhesives of poly(α-lipoic acid). *Science* **385**, 877–883 (2024).
47. Zhang, Q. et al. Dual closed-loop chemical recycling of synthetic polymers by intrinsically reconfigurable poly(disulfides). *Matter* **4**, 1352–1364 (2021).
48. Zhu, J. et al. A novel dynamic polymer synthesis via chlorinated solvent quenched depolymerization. *CCS Chem.* **5**, 1841–1853 (2023).
49. Wang, Y., Sun, S. & Wu, P. Adaptive ionogel paint from room-temperature autonomous polymerization of α-thioctic acid for stretchable and healable electronics. *Adv. Funct. Mater.* **31**, 2101494 (2021).
50. Shi, C. Y., Zhang, Q., Wang, B. S., Chen, M. & Qu, D. H. Intrinsically photopolymerizable dynamic polymers derived from a natural small molecule. *ACS Appl Mater. Interfaces* **13**, 44860–44867 (2021).
51. Gao, Y. et al. A gentamicin-thioctic acid multifunctional hydrogel for accelerating infected wound healing. *J. Mater. Chem. B* **10**, 2171–2182 (2022).
52. Higginson, C. J. et al. Bioinspired design provides high-strength benzoxazine structural adhesives. *Angew. Chem. Int. Ed.* **58**, 12271–12279 (2019).
53. Ma, C. et al. Ultra-strong bio-glue from genetically engineered polypeptides. *Nat. Commun.* **12**, 3613 (2021).
54. Cui, C. et al. A coenzyme-based deep eutectic supramolecular polymer bioadhesive. *Adv. Funct. Mater.* **33**, 2307543 (2023).
55. Xie, X., Xu, X. & Jiang, Y. Hydrogen-bonding interaction-driven catechin assembly into solvent-free supramolecular adhesive with antidrying and antifreezing properties. *ACS Appl. Polym. Mater.* **4**, 4319–4328 (2022).
56. Liu, Y., He, K., Chen, G., Leow, W. R. & Chen, X. Nature-inspired structural materials for flexible electronic devices. *Chem. Rev.* **117**, 12893–12941 (2017).
57. Deng, X. et al. Strong dynamic interfacial adhesion by polymeric ionic liquids under extreme conditions. *ACS Nano* **16**, 5303–5315 (2022).

58. Liang, Y. et al. Low-molecular-weight supramolecular adhesives based on non-covalent self-assembly of a small molecular gelator. *Mater. Horiz.* **9**, 1700–1707 (2022).

Acknowledgements

This work was financially supported by the National Key R&D Program of China (2023YFA1507204, Y.-Q. L.), NSFC (Grants 22225109, Y.-Q. L.; 22071109, S. L. L.; 22171139, Y. C.), Natural Science Foundation of Guangdong Province (No. 2023B1515020076, Y. C.) and Fundamental Research Program of Shanxi Province (20210302124339, X. M. X.).

Author contributions

Y.-Q. L., Y. C. and X.M. X. conceived and designed the idea. X.M. X., R. L., Y. Q. and Y. C. designed the experiments, collected and analyzed the data. X.M. X., Y. Q., J. Z., Z. Z., Y. P., X.Y. X., J. Y., S-L. L. and R. L. papered the experiments and characterizations. R. L. analyzed DFT and MD calculations. X.M. X., R. L., Y. C. and Y.-Q. L. discussed the results and prepared the manuscript. X.M. X. and Y. C. wrote the manuscript.

Competing interests

The authors declare no competing interests.

Additional information

Supplementary information The online version contains supplementary material available at https://doi.org/10.1038/s41467-025-60076-x.

Correspondence and requests for materials should be addressed to Yifa Chen or Ya-Qian Lan.

Peer review information *Nature Communications* thanks Yuta Tsuji and the other, anonymous, reviewer(s) for their contribution to the peer review of this work. A peer review file is available.

Reprints and permissions information is available at http://www.nature.com/reprints

Publisher's note Springer Nature remains neutral with regard to jurisdictional claims in published maps and institutional affiliations.

Open Access This article is licensed under a Creative Commons Attribution-NonCommercial-NoDerivatives 4.0 International License, which permits any non-commercial use, sharing, distribution and reproduction in any medium or format, as long as you give appropriate credit to the original author(s) and the source, provide a link to the Creative Commons licence, and indicate if you modified the licensed material. You do not have permission under this licence to share adapted material derived from this article or parts of it. The images or other third party material in this article are included in the article's Creative Commons licence, unless indicated otherwise in a credit line to the material. If material is not included in the article's Creative Commons licence and your intended use is not permitted by statutory regulation or exceeds the permitted use, you will need to obtain permission directly from the copyright holder. To view a copy of this licence, visit http://creativecommons.org/licenses/by-nc-nd/4.0/.

© The Author(s) 2025